3. Background Emission from the Ground

3.1 Near-Infrared Airglow

A major source of sky background is the airglow in the upper regions of the Earth's atmosphere. The photo on the right shows the airglow at an altitude of about 90 km. It is caused by chemical reactions powered by uv radiation from the sun. The highly excited OH^- radical is produced by the reaction:

$$H + O_3 \longrightarrow OH^* + O_2$$

The de-excitation of the OH radical gives rise to numerous emission lines in the visible and near infrared and it dominates the background emission in the near infrared.

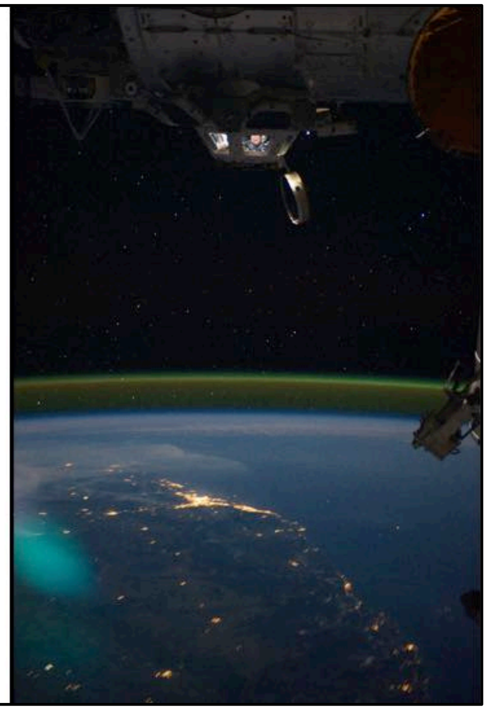

Notes: Figure is from https://spaceflight.nasa.gov/gallery/images/station/crew-28/hires/iss028e050185.jpg.

For a photographic description of airglow: Christensen, L. L., S. Noll and P. Horálek (2016). "Light Phenomena over the ESO Observatories I: Airglow." The Messenger **163**: 40-42.

The figure to the right shows the emissions lines from OH^- and it is the dominant source of sky background emission at 1-2.25 μm.

Note that thermal emission from the sky begins to increase starting at about 1.8 μm.

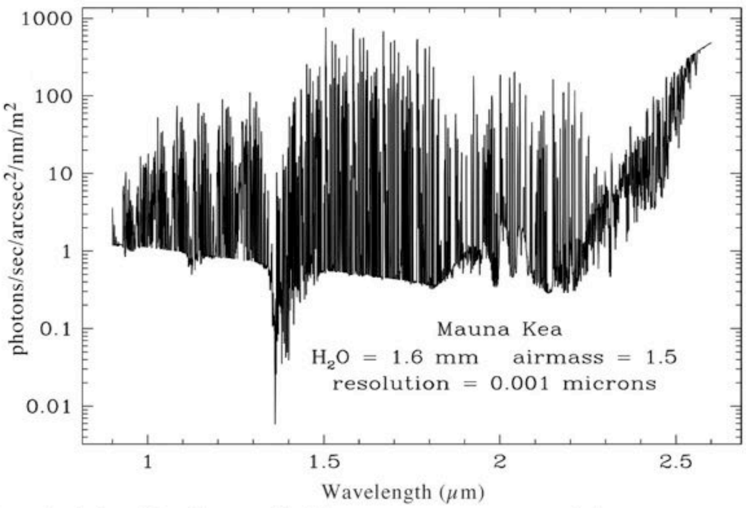

Notes: Figure is from http://gemini.edu/sciops/telescopes-and-sites/observing-condition-constraints/ir-background-spectra.

At very high spectral resolution the individual lines can be resolved and in fact the OH lines are used for wavelength calibration. For example this figure from Rousselot et al. (2000) shows an OH line identification for the purpose of calibrating infrared spectra.

Note that in between the OH lines there is no sky emission and one can expect higher sensitivity in between the OH lines.

Spectrographs that attempt to remove the OH lines have been built, see for example Iwamuro, F. et al. (2001). "OHS: OH-Airglow Suppressor for the Subaru Telescope." Publications of the Astronomical Society of Japan **53**: 355-360.

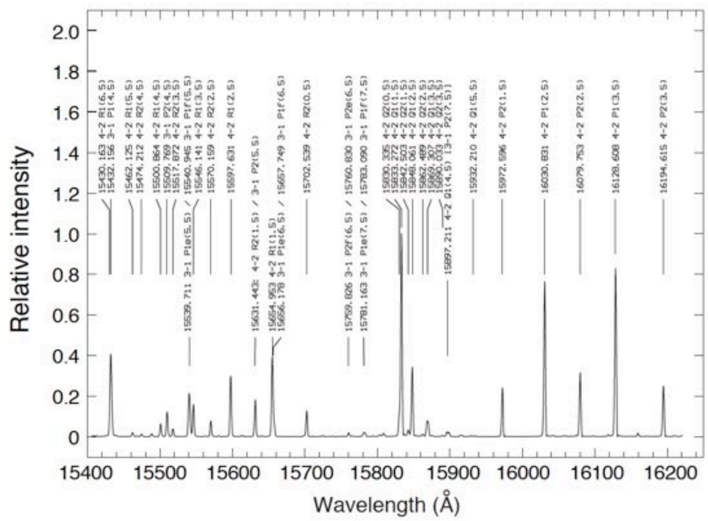

Notes: Figure from: Rousselot, P., C. et al. (2000). "Night-sky spectral atlas of OH emission lines in the near-infrared." Astronomy and Astrophysics **354**: 1134-1150. See also: Oliva, E. and L. Origlia (1992). "The OH Airglow Spectrum - a Calibration Source for Infrared Spectrometers." Astronomy and Astrophysics **254**: 466.

Laboratory OH line positions are given by Maillard, J. P., J. Chauville and A. W. Mantz (1976). "High-resolution emission spectrum of OH in an oxyacetylene flame from 3.7 to 0.9 µm." Journal of Molecular Spectroscopy **63**: 120-141, and by Abrams, M. C. et al. (1994). "High-resolution Fourier transform spectroscopy of the Meinel system of OH." The Astrophysical Journal Supplement Series **93**: 351-395.

This figure shows all sources of background emission (Noll et al. 2014).

There is a “residual continuum” in between the OH lines. This continuum source is believed to arise from an airglow process but it is not understood in detail. It was first discovered by Maihara, T. et al. (1993).

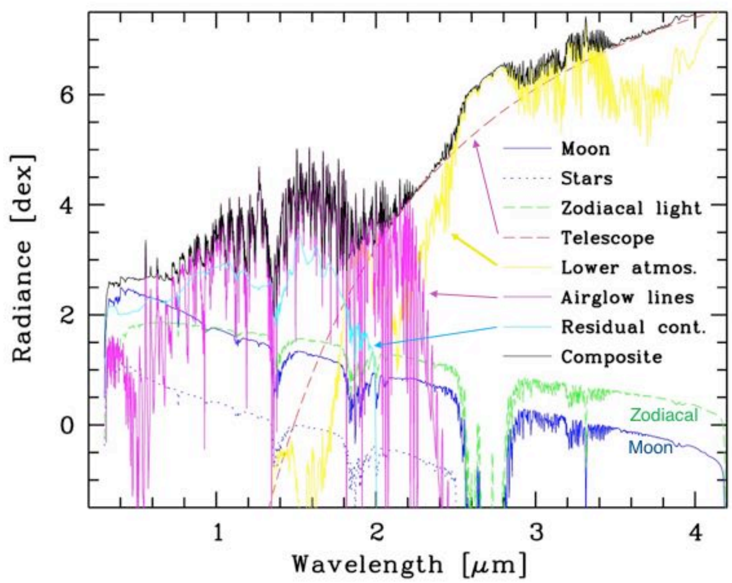

Notes: Figure from: Noll, S., et al. (2014). "Skycorr: A general tool for spectroscopic sky subtraction." Astronomy and Astrophysics **567**.

Note the level of the zodiacal light. In space the zodiacal light is the main source of background emission in the near infrared.

A very detailed discussion of the sky background is given by Leinert, C. et al. (1998). "The 1997 reference of diffuse night sky brightness." Astronomy and Astrophysics Supplement Series **127**: 1-99.

Maihara, T. et al. (1993). "Observations of the OH airglow emission." Publications of the Astronomical Society of the Pacific **105**: 940-944.

The OH emission is not random but arises in groups of emission bands. This is shown here (Noll et al. 2014).

This figure also shows that the OH emission reaches a maximum in the H band.

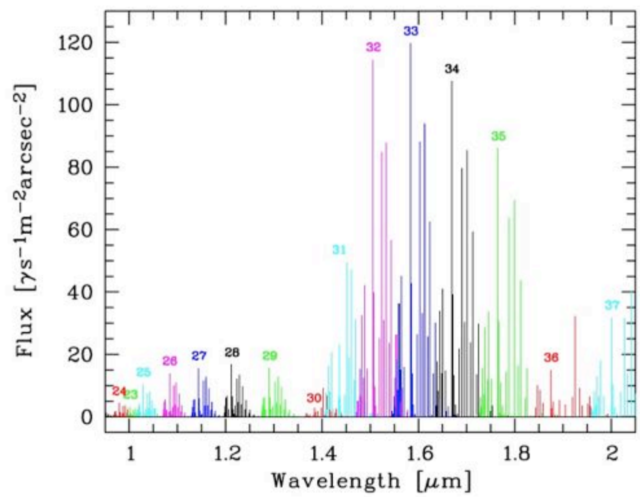

Fig. 5. *A*-group identifications of the OH bands (cf. Table 2) in the wavelength range between 0.95 and 2.05 μm. The wavelengths and zenithal mean fluxes tabulated in the input line list are plotted.

Notes: Figure from: Noll, S., et al. (2014). "Skycorr: A general tool for spectroscopic sky subtraction." Astronomy and Astrophysics **567**.

Note that the OH emission increases with airmass as shown in the figure (Sanchez et al. 2008). This is expected as the path length through the atmosphere increases with airmass. Thus observations are degraded by the higher background and the variability with greater airmass.

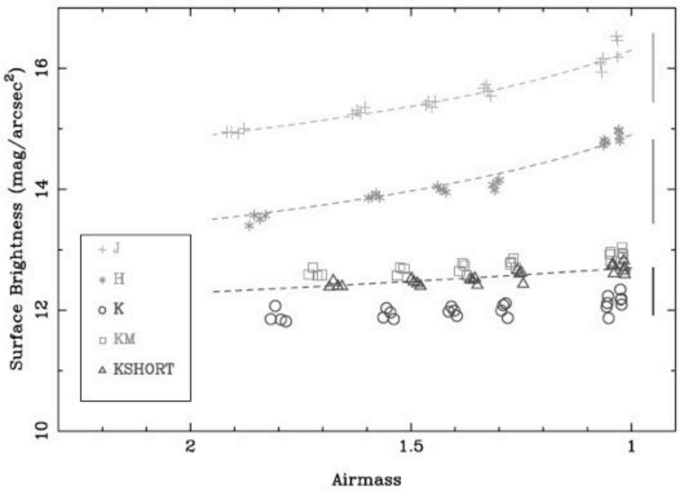

Notes: Figure is from Sánchez, S. F. et al. (2008). "The Night Sky at the Calar Alto Observatory II: The Sky at the Near-infrared." <u>Publications of the Astronomical Society of the Pacific</u> **120**: 1244-1254.

The OH emission drops off at about 2.2 mm. At this wavelength the thermal emission from the telescope is rising rapidly. Therefore at the South Pole there is a small wavelength region, 2.3-2.5 μm where the sky emission is much lower than anywhere else in the world. This is shown in the figure (Phillips et al. 1999). In the next section we will discuss the thermal background.

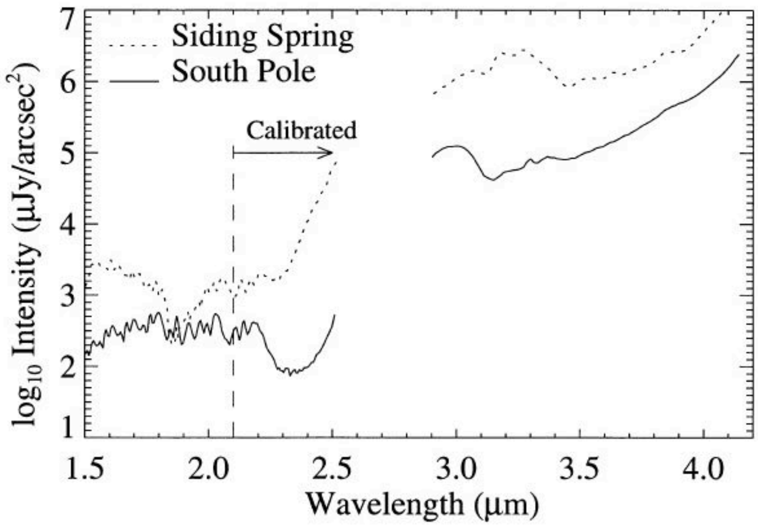

FIG. 15.—Sky emission measured across the *H*, *K* and *L* bands at Siding Spring Observatory in Australia and at the South Pole. A nominal calibration factor has been applied to the data shortward of 2.1 μm.

Notes: Figure from: Phillips, A., M. G. et al. (1999). "The Near-Infrared Sky Emission at the South Pole in Winter." Astrophysical Journal **527**: 1009-1022.

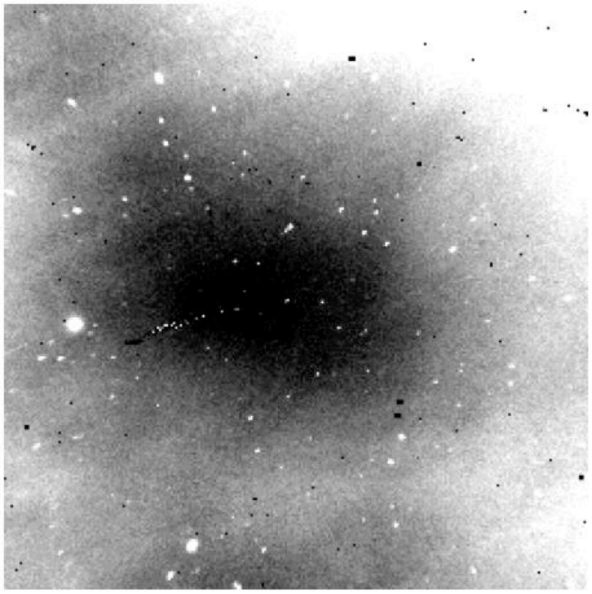

Movie of the OH emission taken by the 2MASS project led by M. Strutskie. This shows what the airglow looks like at 1.6 μm over a period of 1.5 hours. The OH emission varies both spatially and temporally. Variability is as short as a few minutes but there is also long term variability over many years.

Notes: From: http://faculty.virginia.edu/skrutskie/airglow/adams/airglowpage.html "2MASS Airglow Page"

Movie of OH spectral variability made by F. Patat. This movie was made over many days and shows how the spectral lines vary at 4400 - 9000 Angstroms.

Notes: From: http://www.eso.org/~fpatat/science/skybright/ "The Brightness of the Night Sky"

The night sky surface brightness (mag/arcsecond^2), adapted from Sanchez et al. (2008). Note that the South Pole and Mauna Kea are the darkest sites at K_s due to the lower thermal background.

Description	Altitude (m)	Type	*J*	*H*	K_s or *K*
La Palma	2500	Average	15.5	14.0	12.6
Paranal	2635	Darkest	16.5	14.4	13.0
		Darkest	---	---	13.5
Cerro Pachon	2200	---	16.0	13.9	13.5
Mt. Graham	1926	---	---	---	13.5
Mauna Kea	4200	Average	15.6	14.0	13.4
		Darkest	16.75	14.75	14.75
Mt. Hamilton	1283	---	16.0	14.0	13.0
Kitt Peak	2096	---	15.7	13.9	13.1
Anglo-Australian Obs.	1164	---	15.7	14.1	13.5
South Pole	2800	---	16.4	14.7	15.3
		Darkest	16.8	15.2	15.8

Magnitudes given are in the Vega system (that is relative to the flux density from Vega). These are _not_ AB magnitudes.

Notes: Sky brightness due to OH is highly variable. Data from Sánchez et al. (2008), Table 4. South Pole values from Phillips et al. (1999). Kenyon & Storey (2006) expect the South Pole sky brightness to be comparable to other sites, such as Mauna Kea. The cold temperature at the South Pole reduces thermal emission in the *K* band, so the apparent sky brightness is lower than at other sites.

Table is from: Tokunaga, A. T., W. D. Vacca and E. T. Young (2013). Infrared Astronomy Fundamentals. Planets, Stars and Stellar Systems. T. D. Oswalt and H. E. Bond. Dordrecht, Springer Science+Business Media. **vol. 2, Astronomical Techniques, Software, and Data:** 99-174.

Sánchez, S. F. et al. (2008). "The Night Sky at the Calar Alto Observatory II: The Sky at the Near-infrared." Publications of the Astronomical Society of the Pacific **120**: 1244-1254.

Kenyon, S. L. and J. W. V. Storey (2006). "A Review of Optical Sky Brightness and Extinction at Dome C, Antarctica." Publications of the Astronomical Society of the Pacific **118**: 489-502.

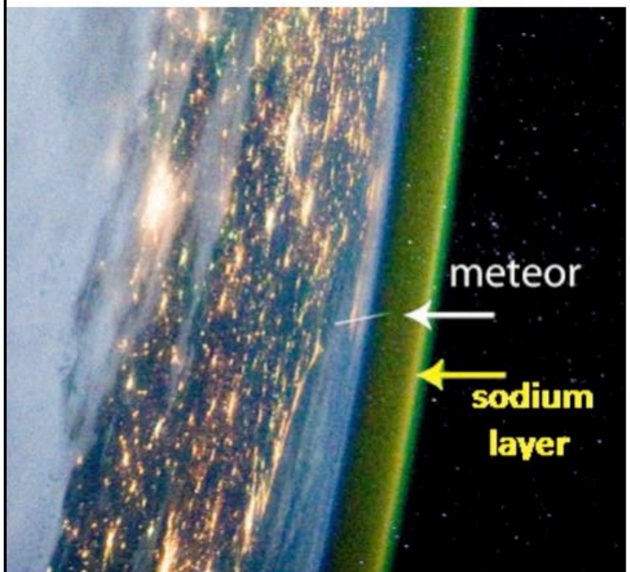

An note about the sodium layer.

At about the same height at the OH radicals is a layer of sodium atoms that comes from the burning up of meteors in the upper atmosphere. This sodium layer does not contribute to the near infrared sky brightness but it is very important for producing artificial guide stars for adaptive optics.

Notes: Image is from: http://www.albany.edu/faculty/rgk/atm101/sodium.htm.

The original image is from: http://auroranightglow.blogspot.com/2012/05/night-glow.html

3.2 Thermal Emission from the Sky and Telescope

Notes: This pair of images illustrate a number of things: (1) Room temperature objects and anything warm is bright in the infrared. (2) There are great differences in transparency between the visible and the IR, like that in dark clouds in the interstellar medium.

Telescope at night. At thermal infrared wavelengths ($\lambda > 2.5\ \mu m$), everything you see in this picture is bright, including the sky.

Notes: The dome, telescope structure, instruments, windows, electronics, and the sky are all glowing at infrared wavelengths. Photo of the NASA Infrared Telescope Facility (IRTF) at Maunakea.

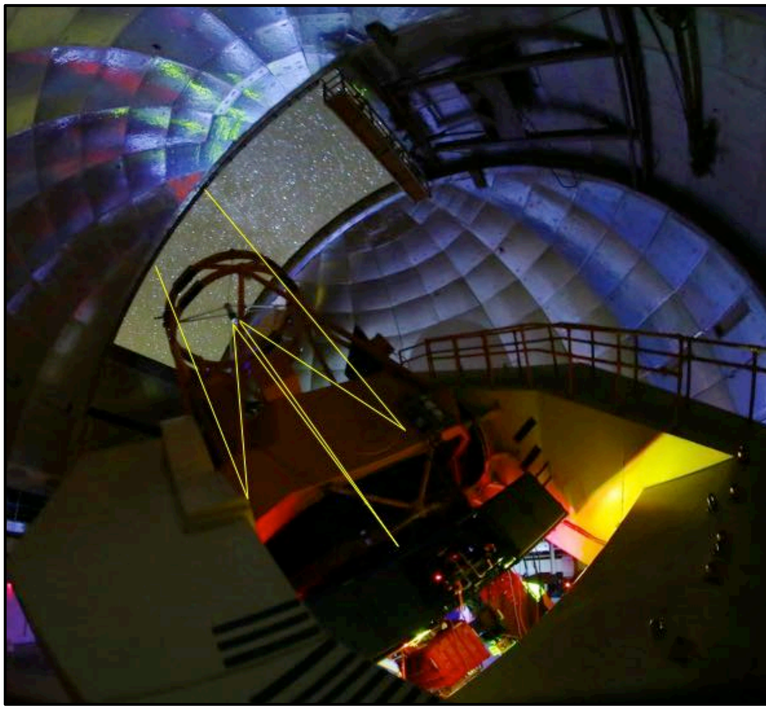

The light path is shown. Since the IRTF was designed to be a low infrared background telescope, the secondary mirror is very small. The focal ratio at the cassegrain focus is f/35. This minimizes the central obscuration and keeps the overall emissivity of the telescope low.

3- 14

Notes: The dome, telescope structure, instruments, windows, electronics, and the sky are all glowing at infrared wavelengths. The equivalent situation in the optical is to observe with the lights on in the dome and having the telescope covered with small light sources. The inside of the dome would also be covered in small lights and the observations would be done in the daytime.

Photo of the NASA Infrared Telescope Facility (IRTF) at Maunakea.

To visualize the thermal emission from the sky and the telescope, imagine putting your eye at the focus of a telescope. Looking upward at the sky you will see the secondary mirror (see figure to the right), which will reflect an image of the spiders, the hole in the primary mirror, and the sky. Each element (including the telescope mirrors) will emit thermal radiation toward the detector. Each item can be approximated by the product of the Planck function and an emissivity factor. For the telescope mirrors and spiders,

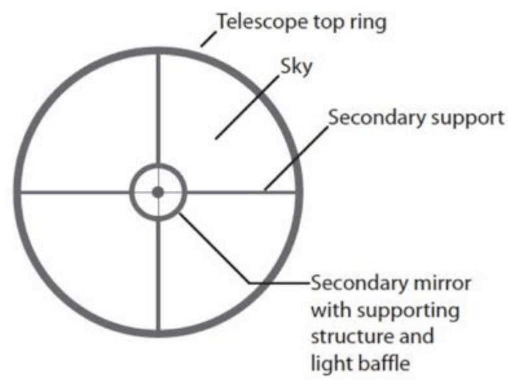

$$Telescope\ Intensity = \varepsilon_{tel} B_\lambda(T_{tel}) A_{tel} + B_\lambda(T_{tel}) A_{spiders} + B_\lambda(T_{tel}) A_{hole} \quad Wm^{-2} sr^{-1}$$

where ε_{tel} is the total emissivity of the telescope mirrors, B_λ is the Planck function, T_{tel} is the telescope temperature, A_{tel} is the telescope area, $A_{spiders}$ is the area of the secondary spiders, and A_{hole} is the area of the hole in the primary mirror.

Notes: Insert Gemini reference for telescope emissivity.

For the sky emission,

$$Sky\ Intensity = (1 - e^{-\tau})B_{\lambda}(T_{sky})A_{tel}$$

where τ is the optical depth of the atmosphere and T_{sky} is the characteristic sky temperature. A good approximation of the characteristic sky temperature at Mauna Kea is 250 K.

The optical depth is typically calculated using a line-by-line atmospheric transmission program such at ATRAN or HITRAN. Note that $(1 - e^{-\tau})$ is the atmospheric absorption and this is an approximation to the emissivity of sky. This is assuming a single slab model for the atmosphere (single layer at constant temperature). In order to have a more realistic accounting of the sky emission a line-by-line calculation and a realistic model of the sky temperature profile is required.

Notes:

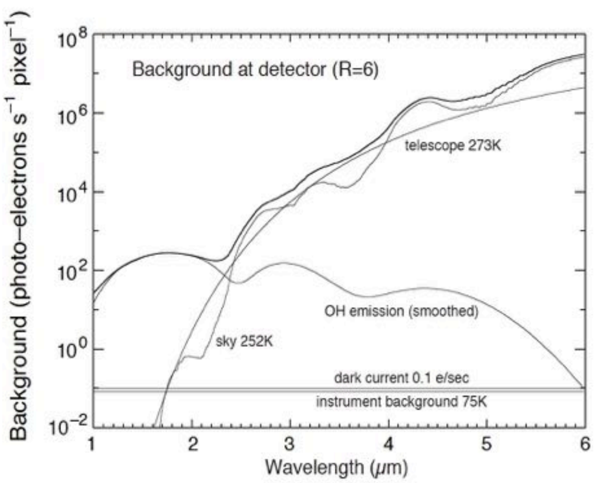

Calculated background from the sky, instrument, and telescope at a resolving power $(\lambda/\Delta\lambda)$ of 6 calculated by J. Rayner. A 3.0-m telescope is assumed, with 0.1 emissivity, telescope temperature of 273 K, sky effective temperature of 252 K, total throughput (telescope, instrument, detector quantum efficiency) of 0.1, pixel size of 0.125", and a slit width of 3 pixels. The emissivity of the sky is estimated as $(1 - e^{-\tau})$ where τ, the atmospheric transmission, was computed from the ATRAN software (Lord, 1992) using an airmass of 1.5 and a precipitable water vapor value of 2.0 mm. The instrument is assumed to be cooled to 75 K, so that the background from the instrument is below that of the dark current.

Notes: This figure is appropriate for broad-band imaging. The aperture assumed for this calculation is not important. What is important is the relative values of the telescope thermal emission, the sky thermal emission, and the OH emission.

This diagram also shows the the detector dark current level and the instrument background when it is cooled to 75K.

The thermal emission from the telescope begins to be larger than the dark current of the detector starting at about 1.7 µm for broadband imaging. This is the wavelength where the telescope thermal emission curve crosses the dark current level in the figure. Instrument cooling is not required for wavelengths less than 1.7 µm. For high-resolution spectroscopy (R = 70,000) the thermal emission from the sky and telescope is greater than the detector dark current for wavelengths greater than 2.5 µm (see Fig. 3-4).

Reference: Lord, S. D. (1992). A new software tool for computing Earth's atmospheric transmission of near- and far-infrared radiation. Moffett Field, CA, Ames Research Center.

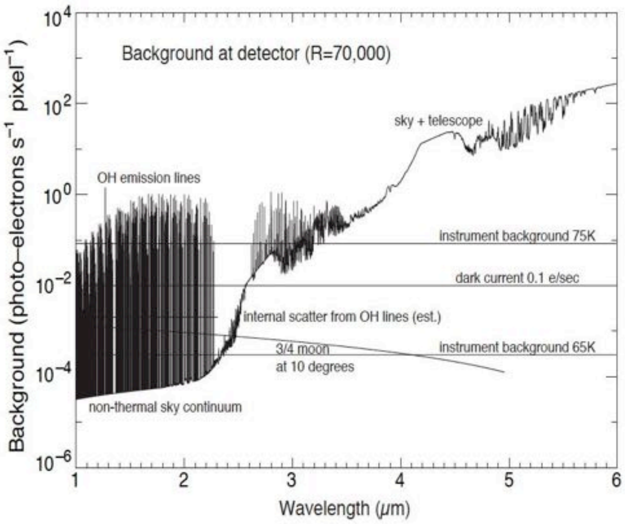

Calculated background from the sky, instrument, and telescope at a resolving power ($\lambda/\Delta\lambda$) of 70,000 calculated by J. Rayner. Same parameters as in previous figure. An instrument model was used to estimate the internal scattered light from OH. The instrument is assumed to be cooled to 65 K, so that the background from the instrument is below that of other sources.

Notes: At high resolving power the thermal emission from the background is lower and so cooling the instrument to a lower temperature is necessary.

The Moon brightness was scaled from Krisciunas & Schaefer (1991) assuming the color of the Moon is that of a G2V star. This is a rough estimate, and it is well below the level of the dark current and so is negligible.

The OH lines are from McCaughrean, M. J. (1988). "The Astronomical Application of Infrared Array Detectors." Ph. D. Thesis, Univ. of Edinburgh.

The nonthermal continuum emission between the OH lines is from Maihara, T. et al. (1993).

Reference: Krisciunas, K. and B. E. Schaefer (1991). "A model of the brightness of moonlight." Publications of the Astronomical Society of the Pacific **103**: 1033-1039.

Maihara, T. et al. (1993). "Observations of the OH airglow emission." Publications of the Astronomical Society of the Pacific **105**: 940-944.

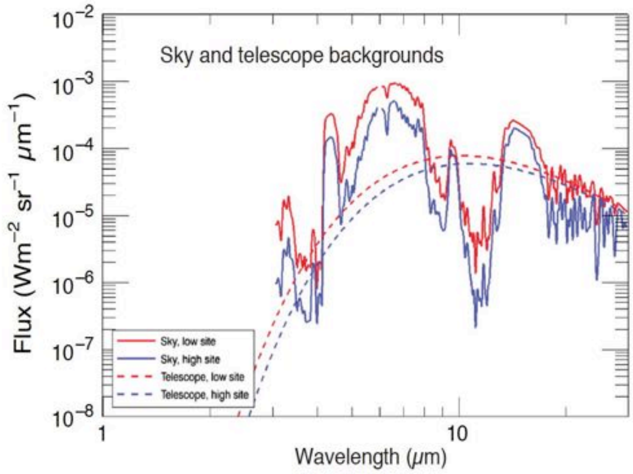

The sky background at mid-infrared wavelengths. Figure shows the sky background at two sites (Kendrew et al. 2010). Instruments working at the mid-infrared are typically cooled to liquid helium temperature (4 K) to keep the instrument thermal emission below that from the sky.

Notes: Kendrew, S. et al. (2010). Mid-infrared astronomy with the E-ELT: performance of METIS. SPIE, San Diego, CA, SPIE.

For an extensive discussion of the sky background, see Leinert, C. et al. (1998). "The 1997 reference of diffuse night sky brightness." Astronomy and Astrophysics Supplement Series **127**: 1-99.

tbd

Notes: